Anti-Spoofing Method for Iris Recognition by Combining the Optical and Textural Features of Human Eye

Eui Chul Lee and Sung Hoon Son
Division of Computer Science, Sangmyung University,
7 Hongji-Dong, Jongno-Gu, Seoul, Republic of Korea
[e-mail: {eclee, shson}@smu.ac.kr]
*Corresponding author: Eui Chul Lee

Abstract

In this paper, we propose a fake iris detection method that combines the optical and textural features of the human eye. To extract the optical features, we used dual Purkinje images that were generated on the anterior cornea and the posterior lens surfaces based on an analytic model of the human eye's optical structure. To extract the textural features, we measured the amount of change in a given iris pattern (based on wavelet decomposition) with regard to the direction of illumination. This method performs the following two procedures over previous researches. First, in order to obtain the optical and textural features simultaneously, we used five illuminators. Second, in order to improve fake iris detection performance, we used a SVM (Support Vector Machine) to combine the optical and textural features. Through combining the features, problems of single feature based previous works could be solved. Experimental results showed that the EER (Equal Error Rate) was 0.133%.

---

1. Introduction

Iris recognition is one of the most secure biometric systems in the world because it uses the unique patterns of the human iris to recognize individuals [1][2]. Most previous research has been focused on iris region segmentation, feature extraction and iris camera systems [1][3][4][5][6][7][8][9]. Recently, it has become important to implement more robust and secure iris recognition systems that can detect and defeat fake irises such as printed, photographed irises, artificial eyes and patterned contact lenses.

Previous research has used one of two methods: the optical feature method, and the textural and material feature method. Initially, the first method was performed by a commercialized iris camera that measured the existence of specular reflections (1st Purkinje images). In this method, an image was generated by a NIR (Near Infra-Red) illuminator that focused on the anterior cornea surface of a live eye. However, it was found that attackers could modify printed iris images by cutting off the printed pupil region and looking through the cut-off hole. This method also produced corneal specular reflections (SR) using the corneal surface of the attacker's eye [10].

In previous research, Lee *et al*. proposed a fake iris detection method that used three Purkinje images [11]. In detail, two features (which represented the distance between the 1st and 4th Purkinje images) and the existence of the 2nd Purkinje image were used. In order to improve performance, they used four features that were the distances between the dual Purkinje images before and after eye rotation, respectively, the size of the 1st Purkinje image and the existence of the 2nd Purkinje image [12]. Also, the SVM (Support Vector Machine) was used to combine the four features and to classify live and fake irises. However, if a fake iris was a semi-transparent patterned contact lens, the system could be spoofed because of the 2nd Purkinje image. Also, since scars on the surface produced an imposter 2nd Purkinje image, some artificial eyes could be falsely accepted as live ones. In addition, user is required to gaze at a camera center and a predetermined position successively, which increased the processing time and user's inconvenience.

Secondly, methods that use textural or material features can be explained as follows. To detect printed iris patterns on a piece of paper or a contact lens, Daugman proposed a method that was based on analyzing the amount of frequency by using the FFT (Fast Fourier Transform) [2][3]. This method measured the high-frequency spectral magnitude of an iris textural area of a captured image, which could be shown periodically for printed iris patterns. Similarly, several researches focused on contact lens with printed iris pattern in which they also performed frequency analysis of iris pattern's texture [13][14][15][16]. However, since high-frequency magnitude could not be measured for blurred fake iris images and printed ones using a high-resolution printer, they were sometimes accepted as live ones. In other research, Lee *et al*. used a variation of the reflectance ratio between the iris and the sclera materials according to infrared light illuminations with different wavelengths [17]. However, this method could not defeat the kinds of patterned lens that showed similar variations of the reflectance ratio between the iris and the sclera regions to that of live irises. Park et al. used a method of multi-spectral fusion of iris textures but it took too much processing time to detect fake irises. Also, patterned lenses were not tested in their research [18]. Other research measured the difference of shadows caused by the 3D structure of the iris texture and the direction of illumination [19]. They performed the wavelet transform and extracted three features such as three differences of standard deviation ($SD1_{hl}$ - $SD2_{hl}$, $SD1_{lh}$ - $SD2_{lh}$, $SD1_{hh}$ - $SD2_{hh}$) (in HL, LH, HH region of wavelet transform) which were obtained from two images

illuminated by the center and side illuminators, respectively. However, this method could not detect some artificial eyes with elaborate 3D iris texture structures.

As mentioned above, since previous research methods have used only one feature between optical [11][12] and textural (material) features [19] of the human eye, these methods have proven to be weak when dealing with specific kinds of fake irises. To overcome these problems and enhance performance, we propose a new fake iris detection method that works by combining the optical and 3D textural features of the human eye. In order to extract optical features, we used the distance between the 1st and 4th Purkinje images (dual Purkinje images). These images were generated on the anterior cornea and posterior lens surfaces, respectively. We did not use the 2nd Purkinje different from because the 2nd Purkinje image can be shown as merged to the 1st Purkinje image due to the structure of eyeball [12]. In addition, different from [12], we measured the distance between the 1st and 4th Purkinje images (dual Purkinje images) only in case that user gazed at the camera center without gazing at the predetermined position, which reduced the processing time and enhanced user convenience.

Also, in order to extract 3D textural features, we measured the changing amount of the iris pattern's shadow with regard to the direction of the illuminator (based on wavelet decomposition). Different from [19] which used three features ($SD1_{hl}$ - $SD2_{hl}$, $SD1_{lh}$ - $SD2_{lh}$, $SD1_{hh}$ - $SD2_{hh}$), we used only one feature ($SD1_{hh}$ - $SD2_{hh}$) of difference of standard deviation of HH region of wavelet transform which were obtained from two images shown by center and side illuminators, respectively. The reason why we use only one feature is that there exist dependency between the ($SD1_{hh}$ - $SD2_{hh}$) and the other two features ($SD1_{hl}$ - $SD2_{hl}$, $SD1_{lh}$ - $SD2_{lh}$). And because we also used the above mentioned optical feature (the distance between the 1st and 4th Purkinje images), we only used one texture feature of ($SD1_{hh}$ - $SD2_{hh}$) in order to reduce the total complexity of combining the optical and textural features.

Consequently, the extracted two features (optical and textural features) were combined with a SVM (Support Vector Machine).

In section 2.1, we present an overview of the proposed method. Then we explain the structure and function of the proposed camera system in section 2.2. Next, we explain the optical and 3D textural features in sections 2.3.1 and 2.3.2, respectively. In section 2.3.3, the SVM classifier that we used to combine two features is discussed. Experimental results and further discussion appear in section 3.

2. Proposed Method

2.1 Overview

The proposed fake iris detection method is depicted in **Fig. 1**.

First, the proposed system captured six iris images by using five IR-LED (Infrared-Light Emitting Diodes) with on and off switches, as shown in **Fig. 1**(a) and **Fig. 3** (2). The five IR-LEDs were called Z-IR, C-IR (L), S-IR (L), C-IR(R) and S-IR(R), as shown in Fig. 3. To avoid large SR (specular reflections) on the glasses' surface, the proposed system selected a pair of images that did not include large SR, as shown in **Fig. 1**(b) and **Fig. 3** (3). Next, the focus status of the selected images was calculated using a focus-measuring mask, as shown in **Fig. 1** (c) [7]. If the focus values were greater than a pre-defined threshold, iris recognition was performed with the enrolled image, as shown in **Fig. 3** (5). When the iris image was successfully identified, the proposed system extracted the 1st feature (F_1) from the dual Purkinje images (1st and 4th Purkinje images) for detecting fake irises based on the optical features of the human eye, as shown in **Fig. 1** (e). Then, the proposed system extracted the 3D

structural features (F_2) of the iris based on wavelet decomposition, which analyzed the changed amount of shadow between a pair of images according to the direction of the illuminator, as shown in **Fig. 1** (f). Then, the extracted two features (F_1 and F_2) were combined using a SVM classifier, as shown in **Fig. 1** (g). If the output of the SVM was close to 1, the input iris image was accepted as a "live iris". If it was close to -1, it was rejected as a "fake iris".
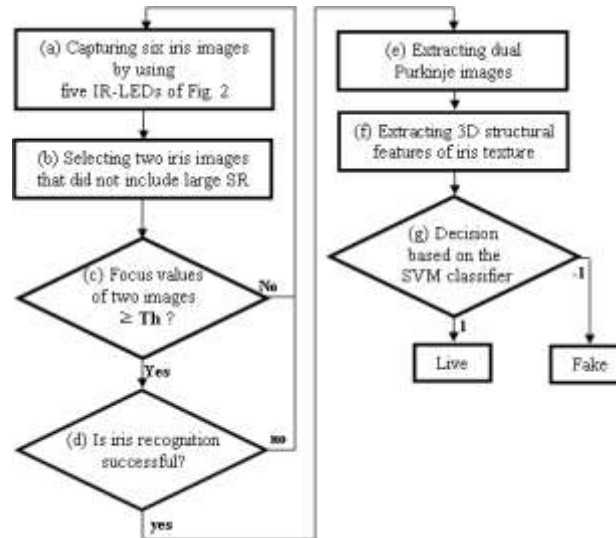

Fig. 1. An overview of the proposed fake iris detection method

2.2 Iris Camera and Controlling Illuminators

To measure the optical and 3D structural features, we used an iris recognition camera with five NIR illuminators, as shown in **Fig. 2**. The C-IR (Central IR), which illuminated the iris in the front, was used for illuminating the iris images that were used for iris recognition and one image for 3D textural analysis of the human eye. The S-IR (Side IR), which illuminated the iris in the side direction, was used for generating the dual Purkinje images and the other image for 3D textural analysis. The two images generated by using the C-IR and the S-IR were B and C (when using C-IR (R) and S-IR (R)) or E and F (when using C-IR (L) and S-IR (L)), as shown in **Fig. 3**. From that information, by comparing the two images acquired by the C-IR and the S-IR, the proposed system carried out 3D textural analysis and used one image from the S-IR for optical analysis.
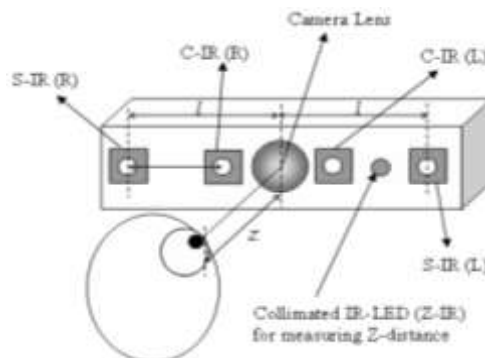

Fig. 2. The structure of the iris camera

Conventional iris recognition camera systems have to address the serious problem of big SR. To solve this problem, we used two sets of two illuminators, (C-IR (R) and S-IR (R)) or (C-IR (L) and S-IR (L)), on the left and right sides of the iris camera, respectively, as shown in **Fig. 3** [21]. In the proposed method, the iris camera captured six iris images by turning on & off five IR-LEDs (Z-IR, C-IR(R), S-IR(R), C-IR(L), S-IR(L)), alternatively, as **Fig. 3**.

In **Fig. 3**, by synchronizing the activation periods of the four IR-LEDs with the output signals of the iris camera (such as the VD (Vertical Drive) signal), we were able to capture six iris images during a very short time period of 198 ms (33ms/image x 6 images). Because the time period between B and C (or E and F) of **Fig. 3** was so small, the conditions of focusing and occlusion (by eyelids and eyelashes) between two images were almost the same.

If a user wore glasses, there may have been big specular reflections (SR) on the glasses surface, as shown in E of **Fig. 3**. However, since the proposed system used two sets of illuminators on the right and left side of the iris camera, as shown in **Fig. 2**, we were able to identify the user if we used B (or C) of **Fig. 3** for iris authentication.

After capturing six iris images, we selected a pair of images with no big SR by counting the pixels (with gray levels greater than 250) in the detected iris region, as shown in **Fig. 3** (3). For example, the proposed system selected the first pair of images (B and C). Then, it calculated the focus values of the selected two images, as shown in **Fig. 3** (4). In brief, we adopted a 5×5 pixel convolution kernel for calculating the focus value of the input iris images. This convolution kernel was originally designed to measure the mid and high-frequency components of the input iris images [7].
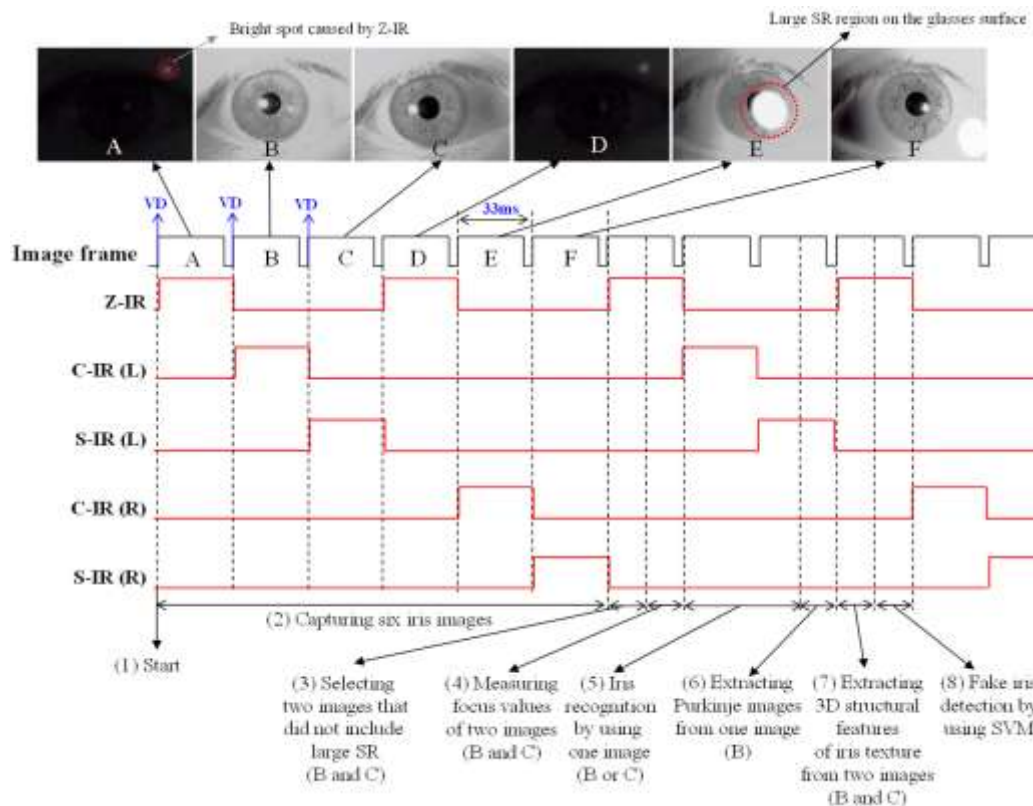

Fig. 3. Camera and illumination control

If the calculated focus values of the two images were lower than the pre-defined threshold, the proposed system captured the six iris images again. If not, it performed iris recognition using one image acquired by the C-IR or S-IR, as shown in **Fig. 3** (5). If iris recognition was successful, the proposed system carried out an optical analysis of one image (B of **Fig. 3**) based on dual Purkinje images (as shown in **Fig. 3** (6)). A detailed explanation appears in section 2.3.1. Then, the proposed system carried out 3D textural analysis by using a pair of images (B and C of Fig. 3) based on wavelet decomposition. Detailed explanations of this procedure are included in section 2.3.2. By using two features (optical and 3D textural features) from the procedure, as shown in **Fig. 3**, the proposed system determined whether the input image was a live iris or not (based on a SVM classifier). Next, in order to measure the Z-distance between the camera lens and the user's eye with A and D of **Fig. 3**, we used one collimated IR-LED (Z-IR) [11][12][20][21]. The Z-IR for measuring the Z-distance was turned on and off before capturing four iris images (B, C and E, F of **Fig. 3**). The measured Z-distance was used for analytic modeling of human eye optics.

2.3 Optical and Textural Features

In this section, we explain optical and 3D textural features. In section 2.3.1, we analytically model the generation of dual Purkinje images based on the human eye structure. And, in section 2.3.2, we explain the anatomical basis of 3D textural features, such as the way that shadows can change according to the direction of illumination.

2.3.1 Optical Features

The human eye has four optical mirror surfaces, each of which reflects bright light: the anterior and posterior surface of the cornea, and the anterior and posterior surface of the lens, as shown in **Fig. 4**. The four reflected images of incident light are called Purkinje images. The positions of these four Purkinje images depend on the geometrical positions of four optical surfaces of the human eye and the light sources [12]. **Fig. 5** (b) is an example of a Purkinje image.
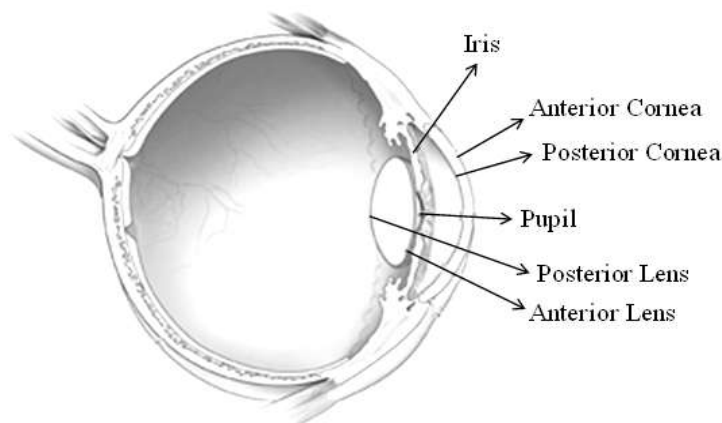

Fig. 4. The optical structure of the human eye [22]

In previous research [12], only the 1st, 2nd and 4th Purkinje images were used to detect fake irises because the 3rd Purkinje image was sometimes hidden by the large 1st Purkinje image. The 2nd Purkinje image was used to detect fake irises in the form of patterned contact lenses. However, since the 2nd Purkinje image was also small, it sometimes was not shown when the captured image was not well focused. In this paper, since the proposed method uses Purkinje

images with 3D textural features, the patterned contact lens can be defeated. So, the proposed method used only the 1st and 4th Purkinje images. These images were referred to as dual Purkinje images.

As shown in **Fig. 5** (a), four Purkinje images were generated from the four optical mirror surfaces [12]. These surfaces included the ACS (Anterior Cornea Surface), the PCS (Posterior Cornea Surface), the ALS (Anterior Lens Surface) and the PLS (Posterior Lens Surface). The dual Purkinje images (1st and 4th Purkinje images) were reflected on the ACS and the PLS. The positions of these Purkinje images depended upon the geometric relationships among the human eye, the illuminator and the camera.
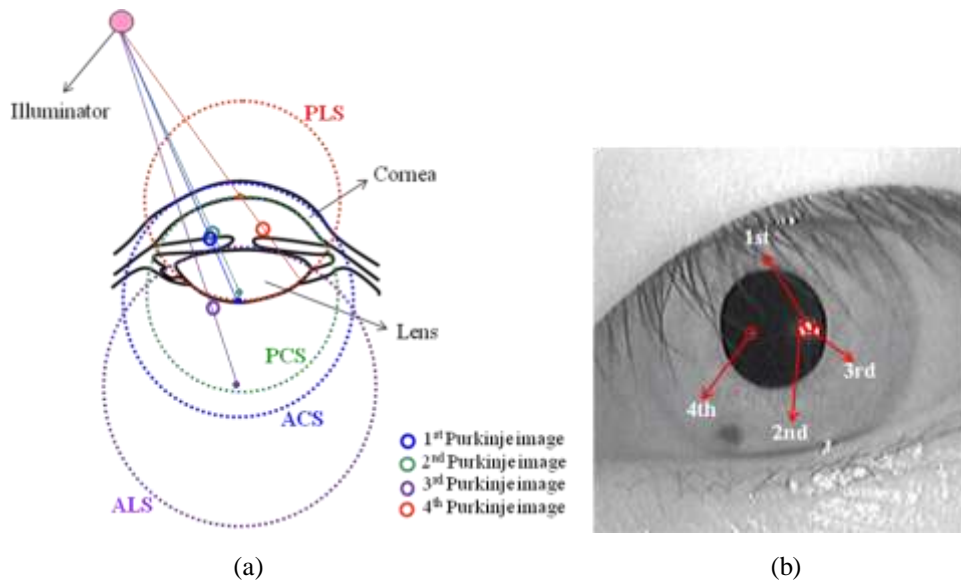

Fig. 5. A conceptual model of a Purkinje image and its example. (a) A conceptual diagram of four Purkinje images. (b) An example of a Purkinje image.

For example, if the distance between the illuminator and the user's gaze position is long, a distance between dual Purkinje images becomes long as shown in **Fig. 6** (b).
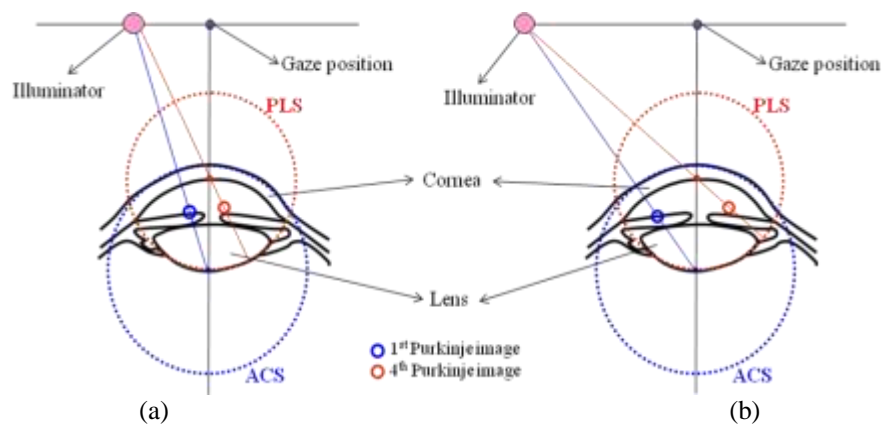
Fig. 6. The change of distance between dual Purkinje images according to distance between illuminator and gaze position. (a) A case of short distance between illuminator and gaze position. (b) A case of long distance between illuminator and gaze position.

Also, even if the distance between the illuminator and the user's gaze position is same, the longer Z-distance between the gaze position and a user's eye causes the shorter distance between the dual Purkinje images as shown in **Fig. 7** (b). Such phenomenon can be explained from the convex mirror theory, also detailed geometric models are described in our previous research [12].
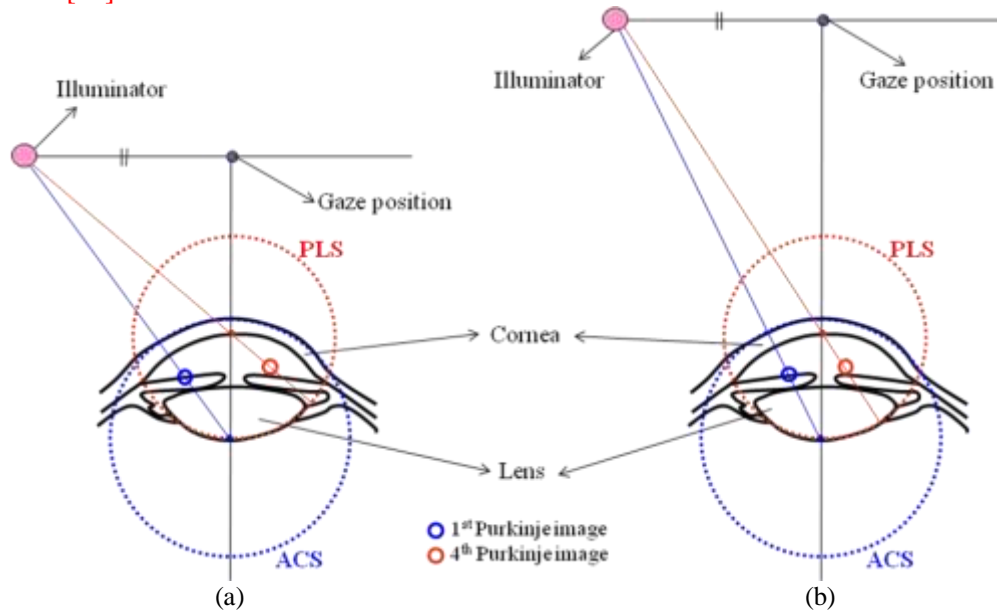
Fig. 7. The change of distance between dual Purkinje images according to Z-distance between illuminator and gaze position. (a) A case of short Z-distance. (b) A case of long Z-distance.

Dual Purkinje images projected onto the camera image plane based on perspective projection can be extracted by using binarization and component labeling because their gray levels are comparatively high than those of iris and pupil region as shown **Fig. 5** (b). Supposing that the positions of dual Purkinje images in acquired iris image are represented as (x_{1st}, y_{1st}) and (x_{4th}, y_{4th}), respectively, Euclidean distance between the 1_{st} and 4_{th} Purkinje images can be calculated. In order to reduce the variations of distance between dual Purkinje images caused by the change of Z-distance between the camera lens and a user's eye, we normalize the calculated Euclidean distance by multiplying the distance between the dual Purkinje images by the Z-distance value (z), as shown in Eq. (1). In Eq. (1), k represents the weight factor that was determined in our experiment.

$$F_1 = k \cdot z \sqrt{(x_{1st} - x_{4th})^2 + (y_{1st} - y_{4th})^2} \tag{1}$$

As shown in **Fig. 8**, there were dual Purkinje images when we used live irises ((a) ~ (c)). In contrast, when we used fake irises, dual Purkinje images were not generated. Also, the measured first feature (F_1) of the fake irises (Eq. (1)) was different from that of the live irises, as shown in **Fig. 8** (d) ~ (f).

In **Fig. 8** (d), although the printed bright circle existed on the pupil boundary, the gray level was lower than that of a genuine Purkinje image. So, by binarization, it could be removed easily. A detailed method for detecting dual Purkinje images is as follows. For patterned contact lenses, such as in **Fig. 8** (g), there were dual Purkinje images that were similar to the live irises. This problem was solved by using 3D textural features, as explained in section 2.3.2.

To detect the position of the dual Purkinje images in the captured image, we used the following method [12]. First, since the iris region was localized by two circular edge detections [8], and the 1st Purkinje image was significantly brighter than the other iris area, we localized the 1st Purkinje image by simple binarization of the iris region. Although the 4th Purkinje image was relatively dark compared to the 1st Purkinje image, because it was in the very dark pupil region, we also detected the 4th Purkinje image by binarization of the pupil region. After that, we obtained the centers of the dual Purkinje images based on component labeling and size filtering.
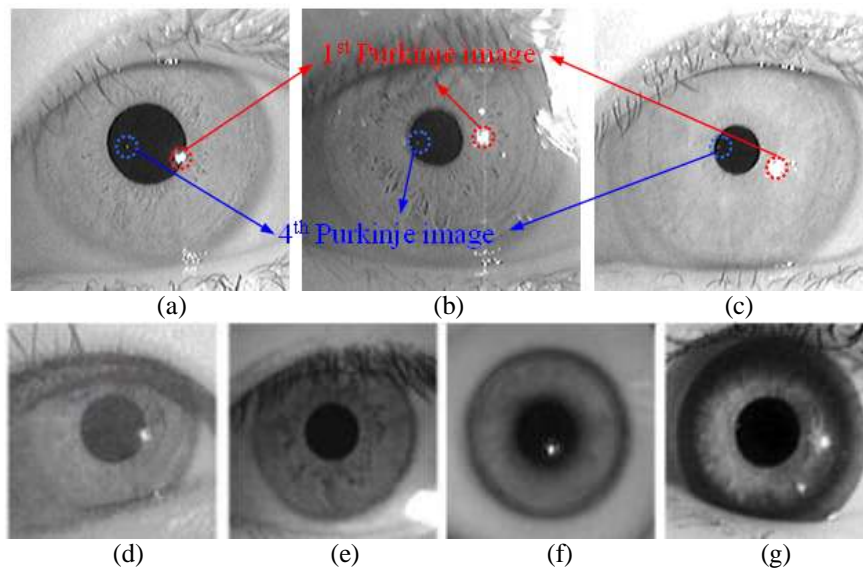
Fig. 8. Sample Purkinje images of live irises ((a) ~ (c)) and fake ones ((d) ~ (g)). (a) Naïve eye. (b) Wearing glasses. (c) Wearing contact lens. (d) Printed. (e) Photograph. (f) 3D acrylic artificial eye. (g) Wearing patterned contact lens.

2.3.2 Textural Features

The basic idea of the proposed method is to measure the changing amount of shadow based on the illumination direction. In detail, we used the fact that more slanted light sources made longer or larger shadows. Also, we could adopt this fact because human iris had the three dimensional intaglio and relief structure as shown in **Fig. 9**.
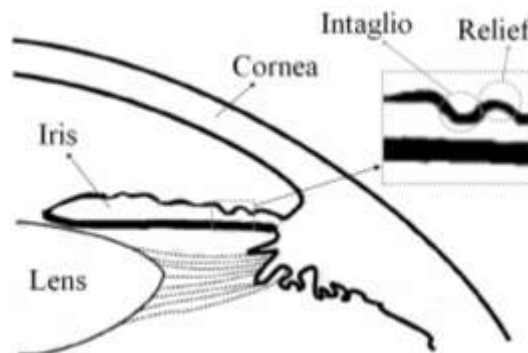

Fig. 9. Three-dimensional structure of the human iris muscle [19][23]

Fig. 10 shows some sample images of live and fake irises that were captured with the proposed iris camera of **Fig. 2**. After comparing the live and fake iris images, we found that the amount of shadow in the iris region when using the S-IR was remarkably greater than when using the C-IR for live irises compared to fake irises.

(a)   (b)

(c)   (d)   (e)
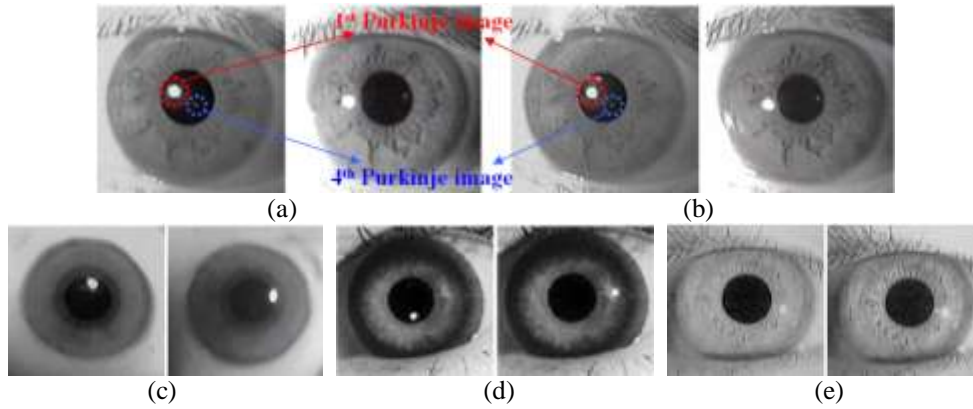
Fig. 10. Samples of two images obtained when using a normal illuminator (C-IR) and a slanted one (S-IR). (a) Naïve eye (live iris). (b) Wearing glasses (live iris). (c) 3D acrylic artificial eye (fake iris). (d) Wearing patterned contact lens (fake iris). (e) Printed image (fake iris).

To discriminate between live and fake irises, we used a feature extraction method based on a wavelet transform. **Fig. 11** shows the results of one-level decomposition based on the Haar wavelet transform.

(a)   (b)   (c)   (d)
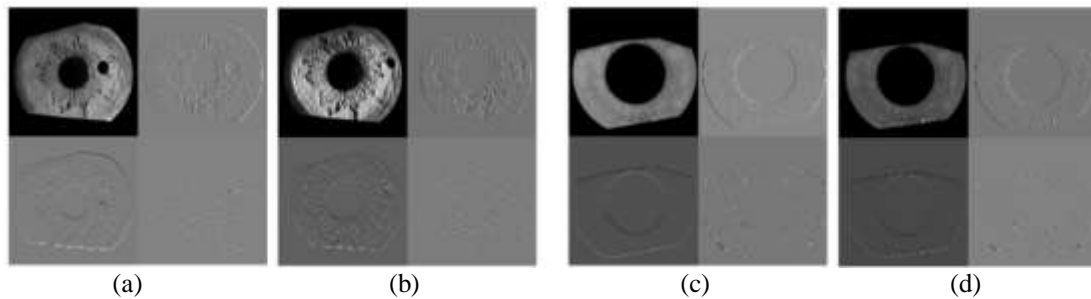
Fig. 11. One-level decomposition images of live and fake irises based on the Haar wavelet transform. (a) and (b) are the live iris images captured with the C-IR and S-IR and decomposed by the Haar filter, respectively. (c) and (d) are the fake iris images (3D artificial eyes) captured with the C-IR and S-IR and decomposed by the Haar filter, respectively.

The fake iris detection procedure when using 3D textural features included three steps. Firstly, we carried out multi-resolution decomposition of the captured two images by using a 2D wavelet transform, as shown in **Fig. 11** [3][19][24]. In (a) ~ (d) of **Fig. 11**, there are four sub regions: LL (low-frequency component in both the horizontal and vertical directions), HL (high and low-frequency component in the horizontal and vertical directions, respectively), LH (low and high-frequency component in the horizontal and vertical directions, respectively), and HH (high-frequency component in both the horizontal and vertical directions). Secondly, we extracted three feature values from the HL, HH, and LH sub-bands of two images by using the C-IR and S-IR (as shown in **Fig. 2**). In our previous research, it was confirmed that the each two standard deviations of HL, HH, and LH sub-bands in respectively captured two

images by the C-IR and the S-IR showed significant differences, because the second image (captured by the S-IR) generated more highlights and shadows due to the 3D structure of iris patterns. In contrast, for the fake samples, the standard deviations of the two captured images were similar. The extracted three features from HL, HH, and LH sub-bands are represented as *SVM* function's three parameters of Eq. (2) [19]:

$$F_2 = SVM(I_1, I_2, I_3) = SVM(SD1_{hl} - SD2_{hl}, SD1_{lh} - SD2_{lh}, SD1_{hh} - SD2_{hh}) \qquad (2)$$

As a final step, single feature is abstracted from the three features such as I_1, I_2, and I_3 of Eq. (2) by using SVM. That is to say, I_1, I_2, and I_3 are adopted as input values of SVM then single output value (F_2) is consequently deduced. Through such abstracting procedure, single value as a 3D textural feature considering three characteristics of sub-bands is generated. Therefore, above extracted optical feature (F_1) and textural feature (F_2) are impartially classified by SVM (see 2.3.3) without inclining to textural feature.

2.3.3 SVM Classification

To combine the optical and 3D textural features (F_1 of Eq.(1) and F_2 of Eq.(2)) of the live and fake samples, we used a SVM (Support Vector Machine). In the past, the SVM has been used to solve two class problems by determining the optimal decision hyper plane. It is based on the concept of structural risk minimization, since it measures the maximum distance to the closest points of the training set. These measurements are known as support vectors [25][26]. For SVM training, we used half the images in the dataset. Detailed explanations about training and test methods are presented in section 3. Two features (F_1 and F_2) were used as the input values of the SVM. The output value of the SVM was represented as a continuous value. A value that was close to 1 represented a live iris and a value that was close to -1 represented a fake one. For the experiment, we used the mySVM [27], which supports linear, quadratic or even asymmetric loss functions. In order to obtain the optimal kernel for the SVM, we compared the classification performances using the RBF (Radial Basis Function), the ANOVA (ANalysis Of VAriance) method, and neural, dot and polynomial kernels with the training data. Five different kernel functions were as follows.

- Radial kernel: $k(x, y) = \exp(-r|x - y|^2)$
- Anova kernel: $k(x, y) = (\Sigma \exp(-r|x_i - y_i|)))^d$
- Neural kernel: $k(x, y) = \tanh(ax*y + b)$
- Dot kernel: $k(x, y) = x*y$
- Polynomial kernel: $k(x, y) = (x*y + 1)^d$

The results showed that performance when using the anova kernel ($r = 0.5$, $d = 4$) was the best.

3. Experimental Results

To measure the accuracy of the proposed method, we acquired several live and fake iris images. We obtained 600 live iris images, which consisted of 20 users that wore contact lenses, 20 users that wore glasses and 20 users that did not wear anything. 10 images were captured from each of these users. Also, we obtained 600 fake iris images, which were placed in six categories: printed irises, photographed irises, printed irises with contact lenses, silicon artificial irises, acrylic artificial irises and pattern printed lenses. Each category contained 10

kinds, and 10 images were captured of each kind. For the experiment, half the live and fake samples were used to train the SVM and the other half were used for testing. We trained using one set of people and tested using a completely different set of people. The compositions of training and test set are as follows:

< Training set >
- Live samples: 30 subjects × 10 samples = 300 samples
- Fake samples: 60 subjects × 5 samples = 300 samples

< Test set >
- Live samples: 30 subjects × 10 samples = 300 samples
- Fake samples: 60 subjects × 5 samples = 300 samples
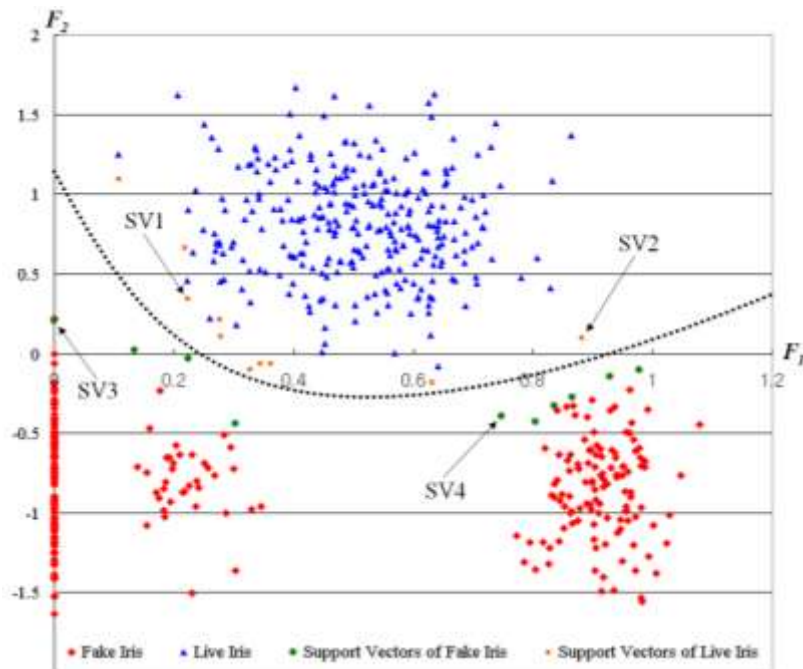
Fig. 12. An example of determined classifier (black solid curve), live and fake irises, 4 samples of support vectors by SVM training

The reason we used half the 60 live subjects for training and the other half for testing was to measure the robustness of the proposed algorithm irrespective of the intra-variation of individual subjects. For the fake samples, because the SVM classifier had to be trained with various kinds of fake samples, the 60 subjects (= 6 categories × 10 kinds) for training are same to those for testing. That is, we used half the 600 samples (= 6 categories × 10 kinds × 5 images) for training and the others (= 6 categories × 10 kinds × 5 images) were used for testing. In our experiments, training and test are five times performed by randomly selecting training and test sets in order to overcome the limitation caused by comparatively small data set.

Fig. 12 shows two dimensional distributions of training data, 4 samples of support vectors, a determined SVM classifier which is acquired using the ANOVA kernel ($r = 0.7, d = 4$). **Fig. 13** shows the real examples of 4 support vectors of **Fig. 12**.
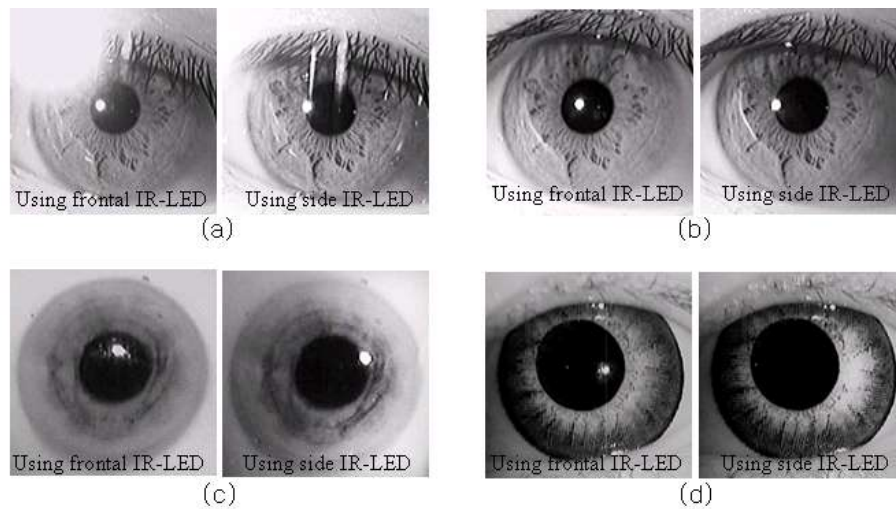
Fig. 13. The real examples of 4 support vectors of Fig. 12. (a) support vector 1, (b) support vector 2, (c) support vector 3, (d) support vector 4.

Fig. 14 shows two dimensional distributions of test data, the determined SVM classifier, one false accepted case and one false rejected case.
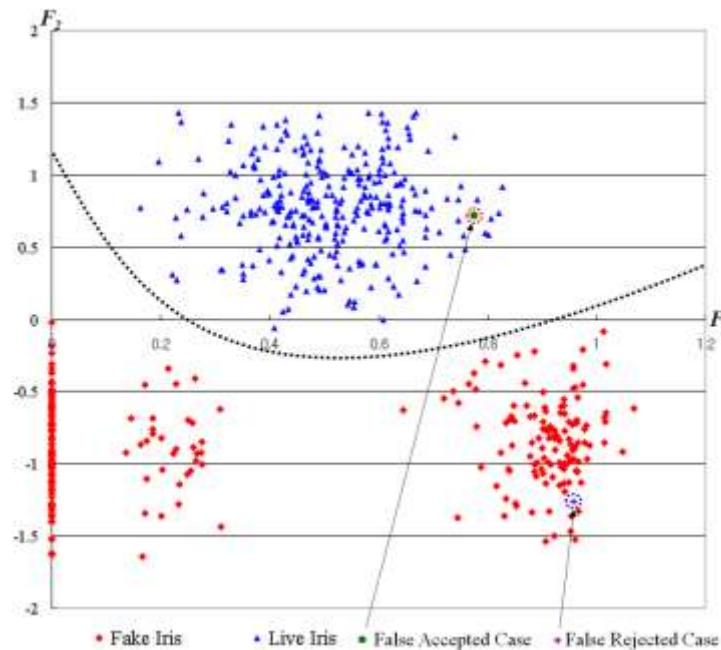
Fig. 14. The determined SVM classifier, one false accepted case and one false rejected case among test data

We then plotted the ROC (Receiver Operational Characteristic) curve using different thresholds with the SVM (Support Vector Machine) classifier, as shown in **Fig. 15**. Based on the two distributions of live and fake samples that were obtained from the output of the SVM, we obtained the ROC curve according to the given threshold. For testing, we used the other images: 300 live samples and 300 fake samples. In order to increase the credibility of the

results, we repeated the experiment twice by interchanging the training and testing sets. Based on the measured average error rate, we plotted the ROC curve and obtained an EER, as shown in **Fig. 15** and **Table 1**. Experimental results showed that the accuracy when using the SVM was superior to single feature-based methods such as F_1 and F_2, as discussed in Eq. (1) and (2).

In addition, we compared the accuracy of proposed SVM fusion method to other score fusion method such as SUM, Weight SUM, Min and Max methods [28] as shown in **Fig. 15**. Though F_1 (Eq.(1)) are F_2 (Eq.(2)) were the extracted feature value, they were used for score value to determine the live or fake iris in [11][12][19]. So, we compared the accuracy of proposed method to other score fusion method.

And we also compared the accuracy of proposed SVM fusion method to other decision level fusion method such as AND or OR rule. **Fig. 15** shows that the proposed SVM based fusion method shows better accuracy compared to other method including only using F_1 or F_2. In **Fig. 15**, the ROC curve of each method was plotted according to the highest order of accuracy.
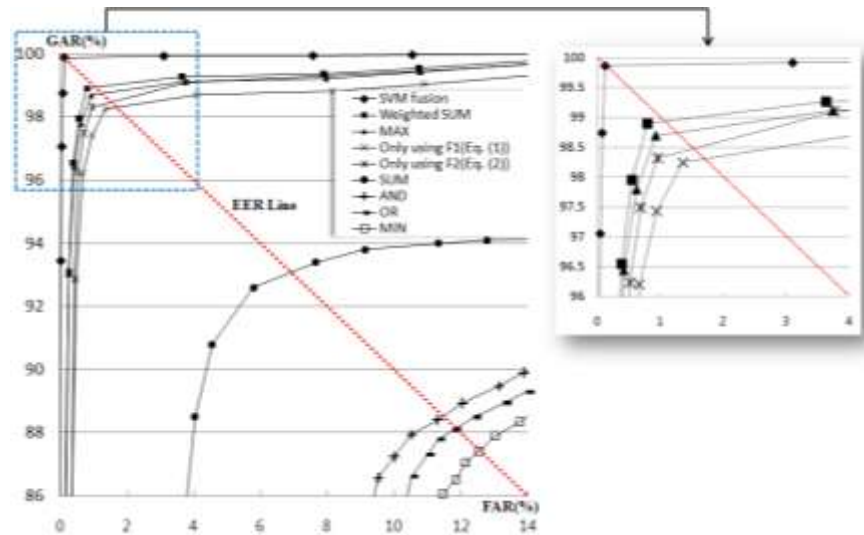

Fig. 15. ROC curves when comparing various kinds of fusion method (GAR = 100-FRR (%))

The EERs of various kinds of fusion method including proposed method were also shown in **Table 1**.

Table 1. EER when comparing various kinds of fusion method (unit : (%))

	SVM Fusion	Weighted SUM	MAX	F_1 ((Eq.(1))	F_2 ((Eq.(2))	SUM	AND	OR	MIN
EER	0.133	1.048	1.250	1.676	1.504	6.910	11.367	11.936	12.512

For measuring the accuracy of our fake iris detection algorithm, we observed two kinds of error rate such as FAR (False Acceptance Rate) and FRR (False Rejection Rate), respectively. Here, the FAR means the error rate of accepting the fake iris as the live one. And the FRR does the error rate of rejecting the live iris as the fake one. The consequent FAR and FRR when

using the SVM were both 0.133% (2/1500) as shown in **Table 1**. Two FARs and two FRRs are respectively occurred from the same samples during different test round. One false acceptance case of **Fig. 14** occurred when working with the patterned contact lens. The semi-transparency of the pattern created an imposter Purkinje image. Also, the visible live iris patterns beneath the semi-transparent lens surface changed the amount of shadow as shown in **Fig. 16** (a). Also, one false rejection case of **Fig. 14** happened when a user was wearing glasses. In detail, a big SR (Specular Reflection) on the glasses surface hid the 1st Purkinje image as shown in **Fig. 16** (b). This meant that the F_1 value could not be measured.

(a)   (b)
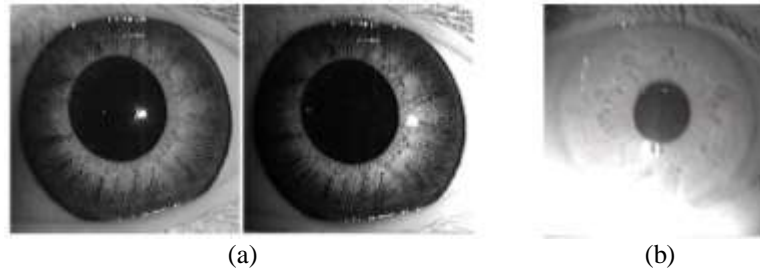
Fig. 16. Examples of false classified samples. (a) False accepted fake sample using patterned contact lens (Left and right images are respectively captured using frontal IR-LED and side IR-LED). (b) False rejected live sample wearing glasses having big SR on the glasses surface.

In the next test, we measured the error rate according to the Z-distance between the eye and the camera. Experimental results showed that the EER did not increase according to the change of Z-distance within the given Z distance operating range (20cm ~ 40cm).
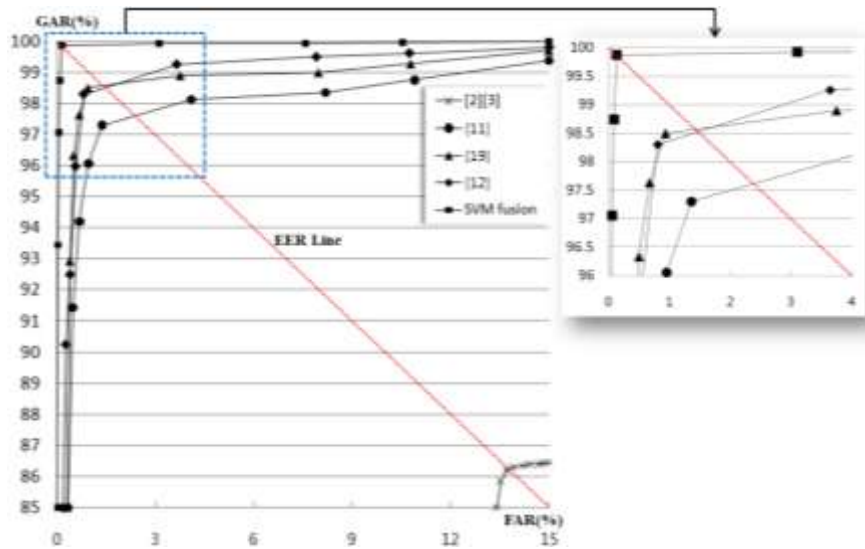
Fig. 17. ROC curves when comparing previous methods (GAR = 100-FRR (%))

The EER when only using F_1 (Eq.(1)) was greater than the EER obtained in previous works [11][12], since we did not use the 2nd Purkinje image when using F_1 (Eq.(25)). The EER when only using F_2 (Eq.(2)) was also greater than that in [19], since three features from the wavelet decomposition images were used in [19] whereas we used only one feature.

Finally, we compared the accuracy of our method to the accuracies of previous ones as shown in **Fig. 17** and **Table 2**.

Table 2. EER when comparing previous methods (unit : (%))

	Fourier-based method of Daugman [2][3]	[11]	[12]	[19]	Proposed SVM fusion
EER	13.79	2.33	1.48	1.41	0.133

As shown in **Fig. 17** and **Table 2**, the proposed method showed the best performance. As shown in Introduction, to detect printed iris patterns on a piece of paper or a contact lens, Daugman proposed a method that was based on analyzing the amount of frequency by using the FFT (Fast Fourier Transform) [2][3]. This method measured the high-frequency spectral magnitude of an iris textural area of a captured image, which could be shown periodically for printed iris patterns. However, since high-frequency magnitude could not be measured for blurred fake iris images and printed ones using a high-resolution printer, they were sometimes accepted as live ones. In our test, they could not detect artificial eye and photographed fake irises.

The processing time of proposed method was only 233 ms (198ms for capturing four images + 35ms for processing) when using a 3.0 GHz Pentium Ⅳ.

4. Conclusion

In this paper, we have proposed a new fake iris detection method that combined the optical and 3D textural features of a human eye. Experimental results showed that the EER was 0.133%. Our proposed method has dependency with the special design of iris camera, our method has following disadvantages. Firstly, in case of specular reflections using both two IR-LEDs of left and right sides, six iris images should be captured again. If the reflective image is used for detecting fake iris, the live iris image can be falsely rejected as fake one. Secondly, in case of severely blurred iris image, the 4th Purkinje image cannot be detected because the theoretical 4th Purkinje image is very small. Thirdly, in case of using fake iris type of semi-transparent patterned contact lens, the 1st and the 4th Purkinje images can be generated like live iris, also iris texture can be similarly analyzed with live iris image. In that case, the fake iris can be falsely accepted as live one. To improve performance and solve above mentioned problems in the future, we will combine another fake iris detection methods based on the pupil dilation / erosion by visible light or multi-wavelength response of iris and sclera.

References

[1] J. G. Daugman, "High confidence visual recognition of personals by a test of statistical independence," *IEEE Transactions on Pattern Analysis and Machine Intelligence*, vol.15, no.11, pp.1148-1160, 1993. Article (CrossRef Link)
[2] http://en.wikipedia.org/wiki/Iris_recognition (accessed on May 25, 2012).
[3] J. G. Daugman, "Demodulation by complex-valued wavelets for stochastic pattern recognition," *International Journal of Wavelets, Multi-resolution and Information Processing*, vol.1, no.1, pp.1-17, 2003. Article (CrossRef Link)
[4] B. J. Kang and K. R. Park, "A robust eyelash detection based on iris focus assessment," *Pattern Recognition Letters*, vol.28, issue.13, pp.1630-1639, 2007. Article (CrossRef Link)
[5] Y. K. Jang, B. J. Kang and K. R. Park, "Robust eyelid detection for iris Recognition," *Journal of*

Institute of Electronics Engineers of Korea, vol.44, pp.99-107, 2007.
http://www.dbpia.co.kr/Article/644160

[6] K. R. Park, H. A. Park, B. J. Kang, E. C. Lee and D. S. Jeong, "A study on iris localization and recognition on mobile phone," *Eurasip Journal on Advances in Signal Processing*, vol.2008, pp.1~12, Nov.2007. Article (CrossRef Link)

[7] B. J. Kang and K. R. Park, "Real-time Image restoration for iris recognition systems," *IEEE Transactions on Systems, Man and Cybernetics - Part B*, vol.37, no.6, pp.1~13, 2007. Article (CrossRef Link)

[8] D. H. Cho, K. R. Park, D. W. Rhee, Y. G. Kim and J. H. Yang, "Pupil and iris localization for iris recognition in mobile phones," in *Proc. of SNPD 2006*, pp.197-201, 2006.

[9] H. A. Park and K. R. Park, "Iris recognition based on score level fusion by using SVM," *Pattern Recognition Letters*, vol.28, issue 15, pp.2019-2028, 2007. Article (CrossRef Link)

[10] B. Toth, "Biometric liveness detection," *Information Security Bulletin*, vol.10, pp.291-297, Oct.2005. Article (CrossRef Link)

[11] E. C. Lee and K. R. Park, "Fake iris detection by using purkinje image," *Lecture Notes in Computer Science*, vol.3832, pp.397~403, 2006. Article (CrossRef Link)

[12] E. C. Lee, Y. J. Ko and K. R. Park, "A fake iris detection method using purkinje images based on gaze position," *Optical Engineering*, vol.47, no.6, pp.067204-1~067204-16, Jun.2008. Article (CrossRef Link)

[13] X. He, S. An, and P. Shi, "Statistical texture analysis based approach for fake iris detection using support vector machine," *Lecture Notes in Computer Science*, vol.4642, pp.540–546, 2007. Article (CrossRef Link)

[14] Z. Wei, X. Qiu, Z. Sun, and T. Tan, "Counterfeit iris detection based on texture analysis," in *Proc. of the 19th International Conference on Pattern Recognition*, pp.1–4, 2008. Article (CrossRef Link)

[15] Z. He, Z. Sun, T. Tan, and Z. Wei, "Efficient iris spoof detection via boosted local binary patterns," *Lecture Notes in Computer Science*, vol.5558, pp.1087–1097, 2009. Article (CrossRef Link)

[16] H. Zhang, Z. Sun, and T. Tan, "Contact lens detection based on weighted LBP," in *Proc. of the 20th International Conference on Pattern Recognition*, pp. 4279–4282, 2010. Article (CrossRef Link)

[17] S. J. Lee, K. R. Park, and J. Kim, "Robust fake iris detection based on variation of the reflectance ratio between the iris and the sclera," in *Proc. of Biometrics Symposium 2006*, Sept.19-21, 2006. Article (CrossRef Link)

[18] J. H. Park and M. G. Kang, "Multi-spectral iris authentication system against counterfeit attack using gradient based image fusion," *Optical Engineering*, vol.46, issue 11, pp. 117003-1~117003-14, Nov.2007. Article (CrossRef Link)

[19] E. C. Lee and K. R. Park, "Fake iris detection based on three dimensional structure of iris pattern," *International Journal of Imaging Systems and Technology*, vol.20, issue 2, pp.162-166, May.2010. Article (CrossRef Link)

[20] R. Jain, R. Kasturi and B. G. Schunck, *Machine Vision*, McGraw-Hill International Editions, pp.301-302, 1995.

[21] E. C. Lee and K. R. Park, "A robust eye gaze tracking method based on virtual eyeball model," *Machine Vision and Applications*, vol.20, issue 5, pp.319-337, Jul.2009. Article (CrossRef Link)

[22] http://www.afb.org/Seniorsite.asp?SectionID=63&DocumentID=3343 (accessed on May 25, 2012).

[23] A. Muron and J. Pospisil, "The Human Iris Structure and Its Usages," *Acta Univ. Palacki. Olomuc., Fac. Rer. Nat. Physica*, Vol. 39, pp. 87-95, 2000. http://publib.upol.cz/~obd/fulltext/Physica%2039/Physica%2039_07.pdf

[24] L. Semler, L. Dettori and J. Furst, "Wavelet-based texture classification of tissues in computed tomography," in *Proc. of 18th IEEE Symposium on Computer-Based Medical Systems*, pp.265–270, 2005. Article (CrossRef Link)

[25] H. Drucker, C. Burges, L. Kaufman, A. Smola and V. Vapnik, "Support vector regression machines," *Advances in Neural Information Processing Systems*, vol.9, pp.155-161, 1996. http://ece.ut.ac.ir/classpages/F83/PatternRecognition/Papers/SupportVectorMachine/support-vector.pdf

[26] Nello Cristianini, John Shawe-Taylor, 2000, *Introduction to Support Vector Machines and Other*

Kernel-based Learning Method, Cambridge University Press.

[27] http://www-ai.cs.uni-dortmund.de/SOFTWARE/MYSVM/index.html (accessed on May 25, 2012)

[28] A. Ross, A. Jain, J. Z. Qian, "Information Fusion in Biometrics," *Pattern Recognition Letters*, vol.24, no.13, pp.2115–2125, 2003. Article (CrossRef Link)

Eui Chul Lee received a BS degree in Software from Sangmyung University, Seoul, South Korea in 2005. He received MS and Ph.D. degrees in Computer Science from Sangmyung University in 2007 and 2010, respectively. He was Researcher in Division of Fusion and Convergence of Mathematical Sciences at the National Institute for Mathematical Sciences from March 2010 to February 2012. Since March 2012, he has been Assistant Professor in the Division of Computer Science at Sangmyung University, Seoul, Korea. His research interests include computer vision, image processing, pattern recognition, Brain Computer Interface (BCI), and Human Computer Interface (HCI).

Sung Hoon Son received his BS degree in Computer Science and Statistics from Seoul National University, Seoul, Korea in 1991. He received MS and Ph.D. degrees in Computer Science from Seoul National University in 1993 and 1999, respectively. After receiving his doctorate, he worked for the System Software Laboratory of Electronics and Telecommunications Research Institute, Daejeon, Korea, as a Senior Member of Engineering Staff. Currently, he is a member of the faculty in the Division of Computer Science, Sangmyung University, Seoul, Korea. His research interests include Operating System, Virtualization, and Embedded system.